PHYSICAL REVIEW E **80**, 055101(R) (2009)

Measurement of the temperature profile of an exothermic autocatalytic reaction front

J. Martin,[1] N. Rakotomalala,[1] L. Talon,[1] and D. Salin[1,2]
[1]*Univ. Pierre et Marie Curie-Paris6, Univ. Paris-Sud and CNRS Lab FAST, Bat. 502, Campus Univ., Orsay F-91405, France*
[2]*Institut Universitaire de France, Paris, France*

(Received 24 July 2009; published 19 November 2009)

Autocatalytic reactions may propagate as solitary waves, namely, at a constant front velocity and with a stationary concentration profile, resulting from a balance between molecular diffusion and chemical reaction. When the reaction is exothermic, a thermal wave is linked to the chemical front. As the thermal diffusivity is nearly two orders of magnitude larger than the molecular one, the temperature profile spreads over length scales (mm) two orders of magnitude larger than the concentration one. Using an infrared camera, we measure the temperature profiles for a chlorite-tetrathionate autocatalytic reaction. The profiles are compared quantitatively to lattice Bhatnagar-Gross-Krook (BGK) numerical simulations. Our analysis also accounts for the lack of observation of the thermal wave for the iodate arsenous acid reaction.

DOI: 10.1103/PhysRevE.80.055101 PACS number(s): 82.40.Ck, 44.35.+c, 47.55.pb

The motion of interfaces and the propagation of fronts resulting from chemical reactions occur in a number of different areas [1], including population dynamics [2,3], flame propagation [4], and catalysis [5]. It is known that autocatalytic reaction fronts between two reacting species may propagate as solitary waves, namely, at a constant front velocity and with a stationary concentration profile [6–8]. For the latter systems, the fluid left behind the front has a different density from the reactant leading to possible buoyancy-driven instabilities [8]. As these reactions are exothermic, a thermal wave front is usually associated with the concentration one [9–12]. Therefore, autocatalytic reaction fronts can produce solutal and thermal density variations due to concentration and temperature variations, respectively. As thermal diffusion is much faster than concentration diffusion (the ratio of the two is the Lewis number, Le ~ 100), the thermal front spreads over a much larger length scale, typically a few mm compared to hundreds of μm for concentration. Depending on the overall density profile, the solutal and thermal effects, conjugated or antagonist, may lead to various buoyancy-driven chemohydrodynamic instabilities [12]: this issue has been addressed with numerical simulations without heat loss [10] and by taking into account the conducting walls [11]. It is worth noting that a "counterintuitive" chemically driven instability [12] has been predicted for a solutal and thermal stable situation due to the difference between the diffusions of heat and mass. However, testing such a prediction requires a good knowledge of the concentration and of the thermal profiles. If concentration measurements have been routinely used, the access to the temperature field is more difficult due to the small exothermicity of the reactions. Yet such a measurement has been recently obtained with a sophisticated optical method [13] during the occurrence of buoyant instabilities. But, the complexity of the two-dimensional pattern formation made it difficult to analyze the data.

In the present work, we address the issue of determining quantitatively the "base state" of these instabilities, namely, the one-dimensional temperature profile of a stable propagating front, for which the overall effect of solutal and thermal density changes does stabilize the front. For that purpose, we use a sensitive infrared (IR) camera to measure accurately the temperature profile. We first recall the basic equations on exothermic diffusion reaction processes. Then we measure the temperature profile for the chlorite-tetrathionate (CT) autocatalytic reaction [14,15]. We compare quantitatively our data with the basic equations, using lattice Bhatnagar-Gross-Krook (BGK) numerical simulations [17,18]. A quantitative extrapolation of our data to the iodate arsenous acid (IAA) reaction explains why the temperature profile in the IAA reaction is not observable within the accuracy of our device.

The CT reaction has been extensively studied and is well documented [7,14,16]. The reaction is autocatalytic with respect to protons with stoichiometry [16],

$$7\ ClO_2^- + 2\ S_4O_6^{2-} + 6\ H_2O \rightarrow 7\ Cl^- + 8\ SO_4^{2-} + 12\ H^+. \tag{1}$$

The concentrations of products (H^+, SO_4^{2-}, and Cl^-) and reactants ($S_4O_6^{2-}$ and ClO_2^-) are well approximated by the two reaction diffusion equations [14,16]:

$$\frac{\partial \alpha}{\partial t} = D_\alpha \Delta \alpha - \frac{1}{\tau} f(\alpha,\beta), \quad \frac{\partial \beta}{\partial t} = D_\beta \Delta \beta + \frac{1}{\tau} f(\alpha,\beta), \tag{2}$$

where $f(\alpha,\beta)=36(\kappa+7\alpha)\alpha\beta^2$ is the dimensionless reaction rate, $\alpha=[S_4O_6^{2-}]/[S_4O_6^{2-}]_0$, $6\beta=[H^+]/[S_4O_6^{2-}]_0$, and $\kappa=2[ClO_2^-]_0/[S_4O_6^{2-}]_0-7$ (a value $\kappa=1$ was chosen for our experiments). D_α and D_β are, respectively, the mass diffusivity of tetrathionate ions and protons, with the latter being sensitively much larger ($D_\beta/D_\alpha=\delta\simeq 5$) [14], and τ is the reaction time.

This set of equations [Eq. (2)] may be solved by using lattice BGK simulations [17,18]. We found that the two concentrations profiles, α and β, travel at a constant velocity. In the simulations, we varied the parameters of the chemical reaction (τ, D_α, D_β): the velocity of the concentrations verifies quite accurately the velocity found by previous authors [14]: $V_\chi=(13.2\sqrt{\delta}-3.2)\sqrt{D_\alpha/\tau}$, for $\kappa=1$. The corresponding concentration profiles, $\alpha(Z)$ and $\beta(Z)$, are given in Fig. 1 in the moving frame of the chemical wave propagating in the z direction ($Z=z-V_\chi t$). In order to compare simulation units and experimental ones, we can note that the chemical wave velocity in Fig. 1 is 1.86×10^{-2} node per time step.

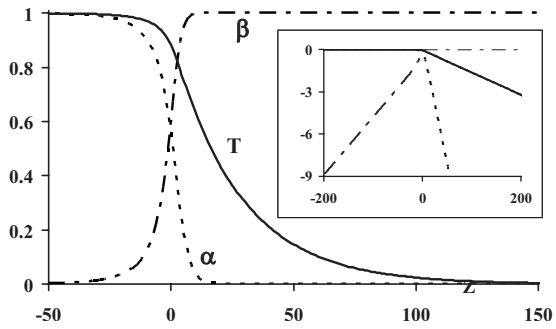

FIG. 1. Lattice BGK simulation of the concentrations, α (dashed line), β (dash-dotted line), and of the normalized temperature T (full line) versus the spatial variable $Z=z-V_\chi t$. Inset: logarithmic-linear plot of the same quantities, emphasizing the exponential decays and growth. The front propagates from left to right. $D_\alpha=10^{-2}$, $D_\beta=5\times10^{-2}$, $D_T=0.7$, and $\tau=2\times10^4$.

As the reaction is exothermic, a temperature solitary wave is linked to the concentration one. Following [11], the temperature field obeys the heat diffusion equation with a source,

$$\frac{\partial T}{\partial t}=D_T\Delta T+\frac{1}{\tau}f(\alpha,\beta)-aT, \tag{3}$$

where D_T is the thermal diffusivity of the solution and T is the temperature rise due to the reaction, normalized by the adiabatic temperature rise, T_a [15] (the one we should get if the whole enthalpy of reaction heated the solution). The last term $-a\ T$ accounts for the heat loss and will be discussed below. Equation (3) is a diffusion equation with sources similar to the concentration ones and it can be also computed with lattice BGK simulations: the corresponding temperature profile $T(Z)$ is given in Fig. 1, without heat loss ($a=0$). It is worth noting that exothermic autocatalytic reactions provide a localized heat source traveling at a constant velocity V_χ [$\partial/\partial t=-V_\chi\partial/\partial Z$ in Eqs. (2) and (3)]. The logarithmic-linear plot of (α, β, T) clearly shows that α and T exhibit exponential decays at large positive Z values whereas β undergoes an exponential growth, for negative Z. These exponential decays and growth are expected from the asymptotics of Eqs. (2) and (3), with respective length scales

$$l_\alpha=\frac{2D_\alpha}{\sqrt{V_\chi^2+144\kappa D_\alpha/\tau}-V_\chi},\quad l_\beta=\frac{D_\beta}{V_\chi},\quad l_T=\frac{D_T}{V_\chi}=\mathrm{Le}\ l_\beta, \tag{4}$$

if the Lewis number is defined with the proton diffusivity. Our numerical simulations show that the validity range of these exponential behaviors corresponds to decades for the concentrations, and thus to a spatial extension much larger than the length scales l_α, l_β. This is of particular interest for the proton concentration β, as the concentration decades correspond to unities of pH, which are easy to measure. Consequently, although the typical value of l_β is very small ($l_\beta\simeq100\ \mu$m and $V_\chi\simeq100\ \mu$m/s, typically [14]), it can be measured with the spatial resolution of a simple "pH paper." We note that the thermal decay length, $l_T\simeq2$ mm, is much larger than the chemical lengths and is suitable for IR camera measurements. Moreover, provided that the Lewis number is known, the measurement of the thermal length could be an alternative measurement of the proton chemical length.

We used the well-characterized exothermic autocatalytic reaction CT, with the classical concentrations of [15] ($[K_2S_4O_6]=5$ mM, $[NaClO_2]=20$ mM, and $[NaOH]=1$ mM) for which the adiabatic temperature rise is $T_a=2400$ mK. A Mach-Zehnder (MZ) optical method enabled us to measure the temperature variations across an unstable front [13]: the MZ method is sensitive to the variations of the refraction index across the whole thickness of the sample and gives the temperature averaged across the gap. The accuracy of about 50 mK requires a rather thick sample (1 mm) [13]. Here, we used an infrared camera (FLIR SC 5500, spectral response of 2.5–5 μm) to follow the development of the thermal wave with a good spatial resolution (about 30 pixels/mm) and a temperature resolution of better than 10 mK. Indeed some care was needed to take advantage of the IR camera. In terms of IR radiance, the aqueous solution is opaque for thicknesses larger than a few tens of microns. Therefore, we measure the temperature of the glass boundary, which is linked to the solution temperature. We note, however, that this limitation is not restrictive for the study of the one-dimensional (along z) regime presented above: it requires, experimentally, a temperature uniform over every cross section of the cell. This can be obtained, using nonadiabatic walls, at small Biot number [19,20], $\mathrm{Bi}=he/\lambda$, with large thermal conductivity (λ) of the thin vessel of thickness e for a heat loss h with the outside on the order of $h\sim10-100$ W/m^2.

A thin glass material fulfills this requirement but the vessel will participate to the total mass to be heated, reducing the expected temperature rise. We used $L=30$-cm-long rectangular cross-section borosilicate glass ($\lambda\simeq1$ W/m-1 k-1) cells of inner width $W=8$ mm and gap thickness $b=0.8$ mm. The wall thickness is identical to the gap width, $e=b$, leading to a Biot number $\mathrm{Bi}\simeq10^{-2}$. Under such conditions, the temperature is uniform in a horizontal plane perpendicular to the front propagation (z, vertical). Note also that we chose a thin enough cell to prevent buoyant instability of the propagation front [15,17]. On the bottom of Fig. 2 the temperature field for the CT reaction is given in a gray scale (color in the online version), with below the corresponding front detected with phenolphtalein as a pH sensitive dye (β measurement). The inset of the figure is a plot of a series of four temperature profiles at four equal time intervals. These profiles, like the concentration profiles measured using the pH sensitive dye, travel with a stationary shape at a constant velocity V_χ. This is verified by the superimposition, in the central part of the figure, of these profiles when plotted in the moving frame ($Z=z-V_\chi t$). Contrary to the predictions without heat loss (Fig. 1), for which a flat temperature profile is followed by an exponential decay, we do observe a traveling wave exhibiting a slow increase, up to a maximal temperature rise T_m followed by a fast decay. This effect is most likely due to heat loss at the surface of the cell (factor h introduced above); therefore, heat loss has to be taken into account. As heat loss is proportional [19,20] to the temperature difference between the cell and the outside, it leads to a

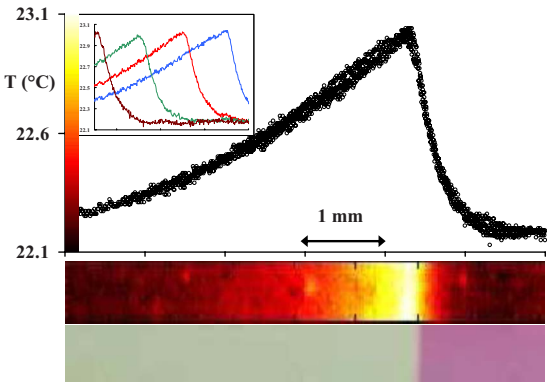

FIG. 2. (Color online) Experiments with the IR camera. Bottom: the front is detected with a pH sensitive dye and propagates vertically upward in the experiments (from left to right, here). Top: temperature field of a 6 cm×8 mm part of the Hele-Shaw cell, with the gray scale (color scale) scale over 1 °C (same range on the vertical axis on the above graph). Inset: thermal wave temperature profiles $T(z)$ at four equal time intervals. Central graph: the same four curves, plotted in the moving frame, $Z=z-V_\chi t$.

"$-aT$" term on the right-hand side of Eq. (3), where a is a coefficient to be determined. In order to fit our data, we have to compute the full Eq. (3). Figure 3 is a plot of a series of lattice BGK simulated temperature profiles for different values of a and the same chemistry [Eq. (2)]. The larger the a, the smaller the maximal height of the peak and the smaller the peak extension along the Z direction.

The middle of Fig. 3 is a logarithmic-linear plot of these profiles: such a plot emphasizes the exponential decay and growth of the temperature for leading ($Z>0$, T_+) and trailing ($Z<0$, T_-) edges of the temperature profiles. Our simulations show that the exponential behaviors extend almost all over the ranges, $0\leq Z<\infty$ and $-\infty<Z\leq 0$. The exponential growth and decay measured in the lattice BGK simulations are the ones expected from the asymptotics of the temperature equation with loss [Eq. (3)], namely,

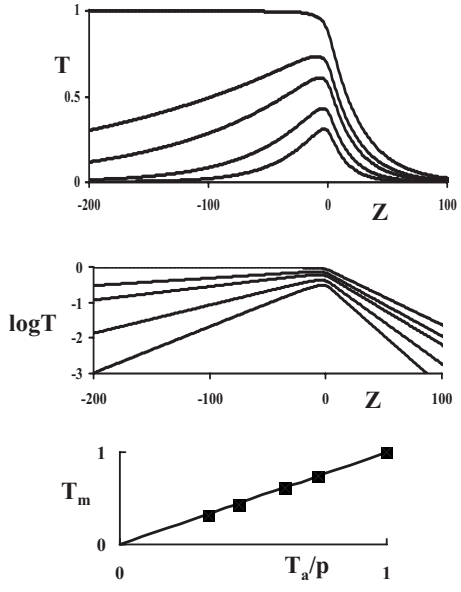

FIG. 3. Lattice BGK simulations of the temperature peak $T(Z)$ with heat loss. Top: linear plot of T versus Z; middle: log $T|$ versus Z. From top to bottom in each figure, the heat loss coefficients are $a=0$, 10^{-4}, 2×10^{-4}, 5×10^{-4}, and 10^{-3}. Bottom: maximal temperature T_m versus T_a/p for the different heat loss coefficients. The straight line corresponds to Eq. (7).

$$T_\pm = T_m e^{\mp Z/l_\pm}, \quad l_\pm = l_T \frac{2}{p \pm 1} \tag{5}$$

with

$$p = \sqrt{1+4a\tau_T}, \quad \tau_T = l_T/V_\chi = D_T/V_\chi^2, \tag{6}$$

where T_m is the maximum of the temperature peak. From the thermodynamic point of view, in our stationary regime, the heat loss flux through the vessel boundaries is equal to the heat flux produced by the reaction, leading to $a\int_{-\infty}^{\infty} T(Z)dZ = V_\chi T_a$, in our notation. Equations (5) and (6) lead then to

$$T_m = T_a/p. \tag{7}$$

The numerical simulations, for different heat loss values (bottom of Fig. 3), are in a good agreement with this relation.

We are now able to interpret our experimental data. We measured the velocity of the thermal wave (as well as the concentration one), $V_\chi = 91\pm3$ μm/s, and the temperature maximum, $T_m = 850$ mK. Note that the latter value is in agreement with thermocouple measurements [15]. The fits to the data (Fig. 2) of the exponential decay and growth give $l_+ = 3.2\pm0.4$ mm and $l_- = 19.1\pm1$ mm. Equation (5) then leads to $l_T = 3.85$ mm and $p = 1.40$, and Eq. (6) leads to $a = 4\times10^{-2}$ s^{-1} and $D_T = 3.5\times10^{-7}$ m^2/s. We may compare the experimental values, so obtained, with modelized equations which account for the heat loss across the solid glass boundaries. The rectangular cross section of the cell has inner sizes $W\times b$ and a wall thickness e equal to the gap, $e=b$. Under the conditions of the experiment (small Biot number), as the temperature is almost the same in the solid and the liquid at a given location (Z), we can compute the effective thermal diffusivity as the ratio of the thermal conductivity to the specific mass of the solid and liquid (weighted by their respective volumes), as well as the maximum temperature,

$$D_T \simeq \frac{(1+2\lambda_s/\lambda_l)D_{Tl}}{1+2\rho_s c_s/(\rho_l c_l)}, \quad T_m \simeq \frac{T_a/p}{1+2\rho_s c_s/(\rho_l c_l)}, \tag{8}$$

where ρ, c, and λ are, respectively, the density, the specific heat, and the thermal conductivity of the glass solid (index s) and solution (index l). $D_{Tl} = \lambda_l/(\rho_l c_l) = 1.4\times10^{-7}$ m^2/s is the solution thermal diffusivity. The thermal quantities where found in [19]. Equation (8) leads to $D_T \simeq 3.2\times10^{-7}$ m^2/s and $T_m \simeq 950$ mK very close to the above experimental values. The heat loss a is the ratio of the product of the heat exchange coefficient h and the area of the cell to the total specific heat of the cell: we get $a \simeq 2h(1+5e/W)/(2e\rho_s c_s + b\rho_l c_l)$. From the experimental value $a \simeq 4\times10^{-2}$ s^{-1} we obtain $h \simeq 100$ W/m^2, in the line with classical values for heat loss [19].

As mentioned in the introduction, the measurement of the concentration profiles requires a probe over decades in con-

centration with a good spatial resolution (on the order of a few tens of microns). A wide range of decades is achievable for pH measurements with a color sensitive dye. With a good calibration of the gray level for the three basic colors (red, green, and blue) of the camera, we achieved a sensitivity of roughly 100 gray levels for a pH variation of 1 unit, i.e., one order of magnitude variation in concentration. The accuracy on the spatial resolution was obtained using a camera with a spatial resolution of typically 4000 pixels/cm. Performing this measurement with different pH indicator papers, we obtained roughly 300 ± 50 μm/(pH unit) corresponding to $l_\beta = 130 \pm 30$ μm. Equation (4) then leads to $D_\beta = (1.2 \pm 0.2) \times 10^{-8}$ m^2/s, in agreement with the values found in the literature [14].

The IR camera technique may be used as well for other exothermic autocatalytic reactions, such as the well-known IAA [6]. Although it is exothermic, this reaction has been reported to barely exhibit any thermal effect [9]. We performed the experiment with the IAA system. We did not detect any heat pulse within our 10 mK resolution. This can be easily understood from the above analysis. The IAA adiabatic temperature rise is only 400 mK and the front velocity is 20 μm/s leading to a factor $p \simeq 5$ and therefore [Eq. (8)] to a maximum temperature peak of 40 mK spreading typically over 2 cm in space (or 1 h in time). Such a measurement would require a control of both the initial temperature and the heat loss far beyond our experimental one. Moreover, such temperature increases generate density variations that are negligible, compared to the ones associated with concentration variations. This explains why the IAA reaction is reported to remain unaffected by temperature effects. And with such an expected temperature profile, it is likely that IAA is not a good candidate for the observation of the chemically driven instability predicted in [12].

In conclusion, using an IR camera we have measured the temperature profiles of the thermal wave associated with an exothermic autocatalytic reaction front. Our data are in quantitative agreement with the theoretical predictions computed with lattice BGK simulations. This experimental tool will be suitable for addressing the solutal and thermal buoyant instabilities in chemical reactions [13,15].

This work benefited from stimulating discussions with Dr. F. Doumenc and G. Gauthier. It was partly supported by CNES Grant No. 8368, ESA (Grant No. AO-99-083), by RTRA "Triangle de la physique," and by the Initial Training Network (ITN) "Multiflow." All these sources of support are gratefully acknowledged.

[1] S. K. Scott, *Oscillations, Waves, and Chaos in Chemical Kinetics* (Oxford University Press, Oxford, 1994).
[2] R. A. Fisher, Proc. Annu. Symp. Eugen. Soc. **7**, 355 (1937).
[3] A. N. Kolmogorov, I. G. Petrovskii, and N. S. Piskunov, Moscow Univ. Math. Bull. (Engl. Transl.) **1**, 1 (1937).
[4] Ya. B. Zeldovitch and D. A. Franck-Kamenetskii, Actu. Phys. USSR **9**, 341 (1938).
[5] S. L. Lane and D. Luss, Phys. Rev. Lett. **70**, 830 (1993), and references therein.
[6] A. Hanna, A. Saul, and K. Showalter, J. Am. Chem. Soc. **104**, 3838 (1982).
[7] S. Szirovicza, I. Nagypal, and E. Boga, J. Am. Chem. Soc. **111**, 2842 (1989).
[8] M. Böckmann and S. C. Müller, Phys. Rev. Lett. **85**, 2506 (2000).
[9] J. Pojman, I. R. Epstein, T. J. McManus, and K. Showalter, J. Phys. Chem. **95**, 1299 (1991).
[10] S. Kalliadasis, J. Yang, and A. De Wit, Phys. Fluids **16**, 1395 (2004).
[11] J. D'Hernoncourt, S. Kalliadasis, and A. De Wit, J. Chem. Phys. **123**, 234503 (2005).
[12] J. D'Hernoncourt, A. Zebib, and A. De Wit, Chaos **17**, 013109 (2007).
[13] P. Grosfils, F. Dubois, C. Yourassowsky, and A. De Wit, Phys. Rev. E **79**, 017301 (2009).
[14] A. Tóth, D. Horváth, and A. Siska, J. Chem. Soc., Faraday Trans. **93**, 73 (1997).
[15] D. Horváth, T. Bánsági, and A. Tóth, J. Chem. Phys. **117**, 4399 (2002).
[16] I. Nagypal and I. R. Epstein, J. Phys. Chem. **90**, 6285 (1986).
[17] J. Martin, N. Rakotomalala, D. Salin, and M. Böckmann, Phys. Rev. E **65**, 051605 (2002).
[18] M. Leconte, J. Martin, N. Rakotomalala, and D. Salin, Phys. Rev. Lett. **90**, 128302 (2003).
[19] F. P. Incropera, D. P. DeWitt, T. L. Bergman, A. S. Lavine, *Fundamentals of Heat and Mass Transfer*, 6th ed. (John Wiley & Sons, Inc., New York, 2006).
[20] N. Özisik, *Heat Conduction*, 2nd ed. (John Wiley & Sons, Inc., New York, 1993).